AMERICAN SOCIETY FOR MICROBIOLOGY | Journal of Virology®

CELLULAR RESPONSE TO INFECTION

Porcine Intestinal Enteroids: a New Model for Studying Enteric Coronavirus Porcine Epidemic Diarrhea Virus Infection and the Host Innate Response

Liang Li,[a] Fang Fu,[a] Shanshan Guo,[a] Hongfeng Wang,[b] Xijun He,[a] Mei Xue,[a] Lingdan Yin,[a] Li Feng,[a] Pinghuang Liu[a]

[a]State Key Laboratory of Veterinary Biotechnology, Harbin Veterinary Research Institute, Chinese Academy of Agricultural Sciences, Harbin, China
[b]Weike Biotechnology, Harbin Veterinary Research Institute, Chinese Academy of Agricultural Sciences, Harbin, China

ABSTRACT Porcine epidemic diarrhea virus (PEDV), a member of the group of alphacoronaviruses, is the pathogen of a highly contagious gastrointestinal swine disease. The elucidation of the events associated with the intestinal epithelial response to PEDV infection has been limited by the absence of good *in vitro* porcine intestinal models that recapitulate the multicellular complexity of the gastrointestinal tract. Here, we generated swine enteroids from the intestinal crypt stem cells of the duodenum, jejunum, or ileum and found that the generated enteroids are able to satisfactorily recapitulate the complicated intestinal epithelium *in vivo* and are susceptible to infection by PEDV. PEDV infected multiple types of cells, including enterocytes, stem cells, and goblet cells, and exhibited segmental infection discrepancies compared with ileal enteroids and colonoids, and this finding was verified *in vivo*. Moreover, the clinical isolate PEDV-JMS propagated better in ileal enteroids than the cell-adapted isolate PEDV-CV777, and PEDV infection suppressed interferon (IFN) production early during the infection course. IFN lambda elicited a potent antiviral response and inhibited PEDV in enteroids more efficiently than IFN alpha (IFN-α). Therefore, swine enteroids provide a novel *in vitro* model for exploring the pathogenesis of PEDV and for the *in vitro* study of the interplay between a host and a variety of swine enteric viruses.

IMPORTANCE PEDV is a highly contagious enteric coronavirus that causes significant economic losses, and the lack of a good *in vitro* model system is a major roadblock to an in-depth understanding of PEDV pathogenesis. Here, we generated a porcine intestinal enteroid model for PEDV infection. Utilizing porcine intestinal enteroids, we demonstrated that PEDV infects multiple lineages of the intestinal epithelium and preferably infects ileal enteroids over colonoids and that enteroids prefer to respond to IFN lambda 1 over IFN-α. These events recapitulate the events that occur *in vivo*. This study constitutes the first use of a primary intestinal enteroid model to investigate the susceptibility of porcine enteroids to PEDV and to determine the antiviral response following infection. Our study provides important insights into the events associated with PEDV infection of the porcine intestine and provides a valuable *in vitro* model for studying not only PEDV but also other swine enteric viruses.

KEYWORDS interferon, porcine epidemic diarrhea virus, PEDV, coronavirus, enteroids, intestine crypt stem cell

The complicated multicellular epithelial surfaces of the intestine contain the primary sites of infection for many gastrointestinal (GI) pathogens and the interfaces for interactions with microorganisms (1, 2). However, fundamental knowledge of intestinal epithelial cell (IEC)-pathogen interactions in pigs is limited due to the lack of a reliable

Citation Li L, Fu F, Guo S, Wang H, He X, Xue M, Yin L, Feng L, Liu P. 2019. Porcine intestinal enteroids: a new model for studying enteric coronavirus porcine epidemic diarrhea virus infection and the host innate response. J Virol 93:e01682-18. https://doi.org/10.1128/JVI.01682-18.

Editor Tom Gallagher, Loyola University Chicago

Address correspondence to Pinghuang Liu, liupinghuang@caas.cn.

L.L. and F.F. contributed equally to this work.

Received 25 September 2018
Accepted 4 December 2018
Accepted manuscript posted online 12 December 2018
Published 19 February 2019

in vitro model that recapitulates the complicated intestinal epithelium *in vivo*. The intestinal epithelium is composed of villi and crypts, and the self-renewing and undifferentiated stem cells in the crypt zone are responsible for the renewal of an entire unit (3, 4). Unlike the classical *in vitro* models of transformed cancer cell lines, enteroids derived from intestinal crypts contain a stem cell niche and diverse highly polarized intestinal epithelial cell types (enterocytes, goblets, enteroendocrine cells, and Paneth cells); thus, these enteroids well mimic the diverse cellular nature and physiological activity of the intestine *in vivo* and represent a new *in vitro* model of infection of the intestinal epithelium by enteric pathogens (5–7). Intestinal enteroids maintain the unique characteristics of the tissue from which they are derived and recapitulate many of the biological and physiological properties of the small intestine *in vivo* (4, 6, 8). As a result, since rodent and human intestinal enteroids were first reported in 2009 and in 2010, respectively, intestinal enteroids have been applied in enteric infection research and have yielded exciting new insights into a variety of aspects of host-virus interactions in the GI tract (4, 7, 9–11). However, enteric infection in porcine intestinal enteroids has not yet been reported.

Porcine epidemic diarrhea virus (PEDV), a member of the alphacoronavirus genus in the family *Coronaviridae*, is the foremost causative agent of acute diarrhea, dehydration, and high mortality rates in seronegative neonatal piglets, which result in substantial economic losses each year (12, 13). PEDV is highly enteropathogenic, primarily infects the villous epithelia of the small intestine, blunts the affected villi, and disrupts mucosal barrier integrity *in vivo* (14, 15). The identity of the specific cell types targeted (enterocytes, goblet cells, Paneth cells, microfold cells, tuft cells, or stem cells) by PEDV infection *in vivo* has remained elusive. However, most *in vitro* studies of PEDV have been performed in nonporcine cell lines, such as Vero cells from African green monkey kidney and HEK293 cells from human embryonic kidney (16–18). Unlike normal mammalian cells, Vero cells are interferon (IFN)-deficient cells that are incapable of producing type I interferons when infected by viruses (19). IPEC-J2 cells, a nontransformed porcine jejunum epithelial cell line from nonsuckling piglets (20), do not mimic the *in vivo* complicated epithelia, and PEDV clinical isolates generally do not replicate very well in porcine nontransformed epithelial cells such as IPEC-J2 cells (21, 22). The absence of a robust experimental *in vitro* system that can recapitulate the *in vivo* PEDV infection process is a bottleneck hampering the investigation of PEDV pathogenesis and the development of novel rational strategies against PEDV infection. Therefore, the development of *in vitro* models that can closely recapitulate the porcine intestine is crucial for expanding the current knowledge of PEDV pathogenesis and facilitating further biological investigations of host-PEDV interactions.

In the present study, we generated crypt cell-derived enteroids and used this model to study PEDV infection. The results revealed that porcine enteroids were susceptible to PEDV infection and recapitulated many of the events associated with PEDV infection in porcine intestines *in vivo*. Collectively, these data illustrate that porcine enteroids, which recapitulate the key properties of the *in vivo* intestinal epithelium, provide an invaluable resource for addressing fundamental aspects of enteric coronaviruses that cannot be modeled using traditional cell lines.

RESULTS

Generation of porcine intestinal enteroids derived from intestinal crypt stem cells. To closely mimic the events associated with enteric virus infection in the swine intestine, we generated primary porcine enteroid cultures derived from piglet intestinal crypts containing leucine-rich-repeat-containing G-protein-coupled receptor 5 (Lgr5)-positive ($Lgr5^+$) stem cells. Crypts from the duodenum, jejunum, or ileum were freshly isolated as described previously, with slight modification, and were cultured in a semisolid, laminin/collagen-rich Matrigel in proliferation medium to allow their differentiation into three-dimensional (3D) enteroids in 7 to 15 days using previously developed methods (4, 11, 23). After a period of approximately 1 to 2 weeks in Matrigel culture, the intestinal crypt cells proliferated and differentiated into 3D enteroids with

a central lumen surrounded by an epithelium containing villus-like structures and budding crypt-like domains, which indicated that the crypt cells from all three small intestine regions could grow into enteroids (Fig. 1A). Because most of the reported enteroid studies have been performed using ileal enteroids, we used ileal enteroids as representative intestinal enteroids and performed most of the experiments of the present study using ileal enteroids. To evaluate whether the differentiated enteroids could be cryopreserved and thawed and whether the resulting thawed cells could differentiate into enteroids, as previously reported, differentiated ileal enteroids were subjected to a freeze-thaw cycle and then differentiated as if they were freshly isolated crypt stem cells. The thawed ileal enteroid single cells grew into enteroids in 7 days (Fig. 1B), and thus, we developed a porcine crypt-derived 3D enteroid culture system.

Because the apical membrane of the 3D enteroids for viral infection faces the inside of the enteroids, infection of 3D enteroids is challenging. We thus sought to develop a porcine planar (two-dimensional [2D]) ileal enteroid culture in microplates, which would make them amenable to efficient infection and would allow deciphering of the complex interplay between viruses and epithelial cells. Previous studies demonstrated that dissociated 3D mouse enteroids can generate planar enteroid monolayers with proper apical and basal polarity that largely recapitulate the many features of 3D enteroids and the *in vivo* intestinal epithelium (23, 24). The 3D ileal enteroids that were expanded in Matrigel were harvested, mechanically dissociated, and seeded on Matrigel-coated microplates to establish 2D enteroids as described previously (24). After expansion and differentiation, the seeded cells grew out as large, contiguous sheets of epithelium with heterogeneity in terms of cell morphology and densities (Fig. 1C). A large number of villin-positive enterocytes were present on the apical surface and throughout the 2D monolayer (Fig. 1D), indicating the presence of mature enterocytes in the enteroids. Proliferating cells stained with Ki-67 protein and stem cells ($Lgr5^+$) were present throughout the 2D monolayers, which suggested that our 2D enteroids maintain the features of stem cells and contain the transit-amplifying zone. We also identified Paneth (lysozyme C-positive [LYZ^+]) cells, goblet (mucin 2-positive [$Muc2^+$]) cells, and enteroendocrine (chromogranin A-positive [$CHGA^+$]) cells in the 2D ileal enteroids (Fig. 1D). Thus, the planar intestinal enteroids generated from budding crypt-like 3D enteroids include multiple cell lineages and recapitulate the various cellular phenotypes of the intestinal epithelium. Moreover, a lumen-like structure was identified in the differentiated planar 2D ileal enteroids (Fig. 1D). Altogether, these results demonstrate that a planar swine enteroid culture can be generated from intestinal crypt stem cells.

Porcine intestinal enteroids are susceptible to PEDV infection. To determine whether porcine intestinal enteroids are permissive to infection by PEDV, we inoculated porcine ileal enteroids with the clinical isolate PEDV-JMS at increasing multiplicities of infection (MOIs). At 48 h postinfection (hpi), the numbers of PEDV genomes were substantially increased to levels 34- to 754-fold higher than their levels at 2 hpi and were correlated with the MOI (Fig. 2A), indicating that PEDV can infect enteroids. It is well established that PEDV primarily infects the small intestine and can infect all three regions (duodenum, jejunum, and ileum) of the small intestine. To assess the potential existence of a disparity in susceptibility to PEDV infection among duodenal, jejunal, and ileal enteroids, we infected the three types of enteroids at the same MOI and monitored the viral replication kinetics. The duodenal, jejunal, and ileal enteroids were all infected by PEDV, and the results showed that the number of PEDV genomes had increased up to 63-fold at 24 hpi compared with the number at 2 hpi and peaked at 48 hpi, indicating successful PEDV replication in all three enteroids. In addition, the enteroids derived from the duodenum, jejunum, and ileum exhibited similar viral replication kinetic levels after PEDV infection (Fig. 2B). PEDV infection in ileal enteroids was further confirmed through an anti-PEDV nucleocapsid immunofluorescence assay (IFA) (Fig. 2C). Successful PEDV infection in ileal enteroids resulted in a significant cytopathic effect and disruption of the enteroid structure starting at 24 hpi, and this structure

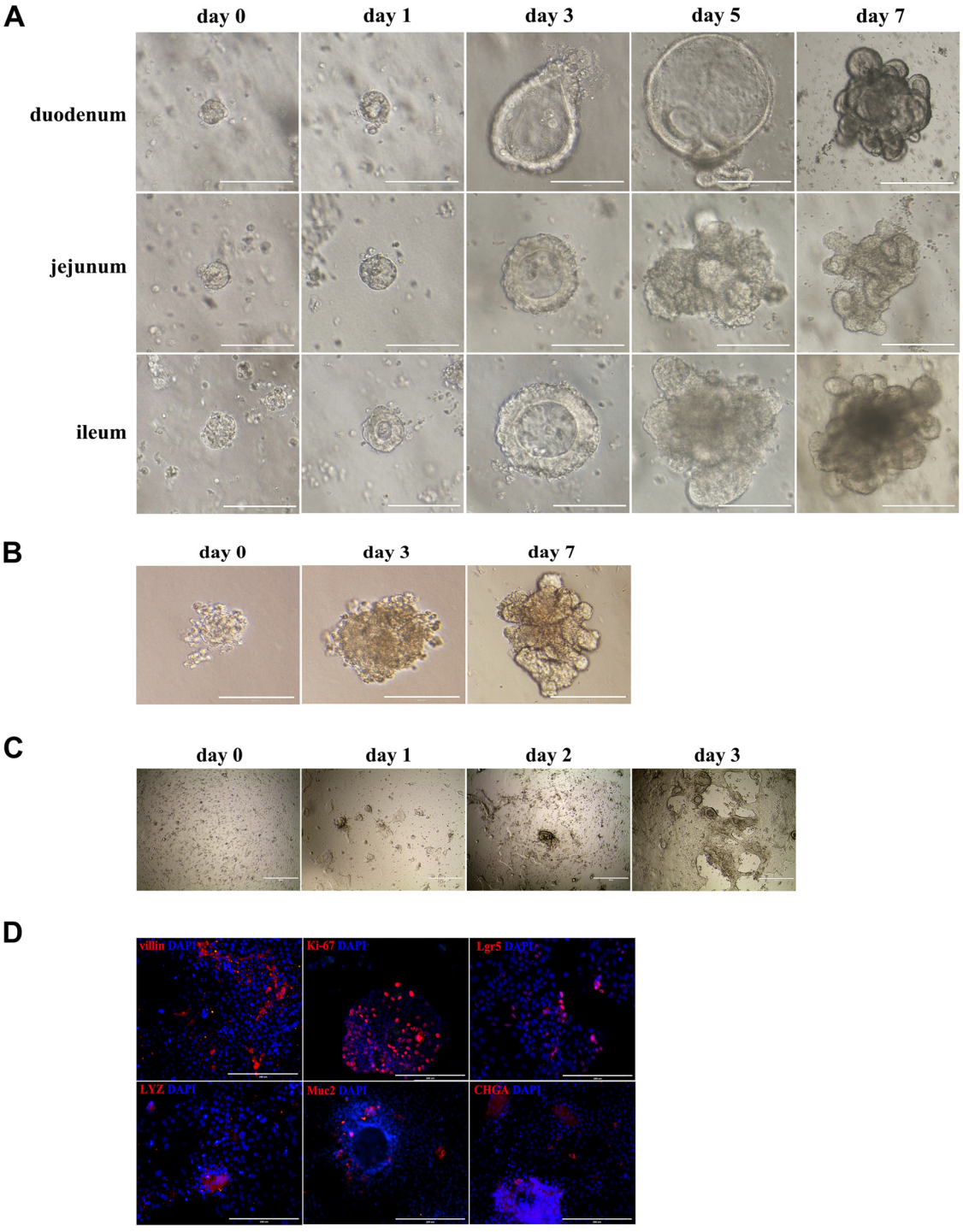

FIG 1 Generation of porcine enteroids derived from intestinal crypt stem cells. (A) Representative images of the time course of porcine enteroid differentiation from intestinal crypts. During culture in Matrigel, small spheroids form on day 3 after crypt isolation, gradually mature over time, and form budding-like crypt structures on day 7. (B) Development of ileal enteroids from frozen-thawed enteroid cells. Enteroids from frozen-thawed enteroid cells were cultured and differentiated as described above for panel A. (C) Representative images of the time course of ileal enteroid monolayers differentiated from enteroid cell plating. Crypt-derived 3D enteroids were enzymatically dissociated into single cells and seeded onto precoated 96-well plates in IntestiCult organoid growth medium to differentiate for 3 days. (D) Identification of different cell lineages in enteroid monolayers. Enteroid monolayer cultures were fixed and costained for specific cell lineages in the porcine intestine using DAPI (nuclear staining) (blue) and surface marker antibodies to Lgr5 for stem cells (red), Ki-67 for proliferating cells (red), villin for enterocytes (red), lysozyme C (LYZ) for Paneth cells (red), mucin 2 (Muc) for goblet cells (red), and chromogranin A (CHGA) for enteroendocrine cells (red).

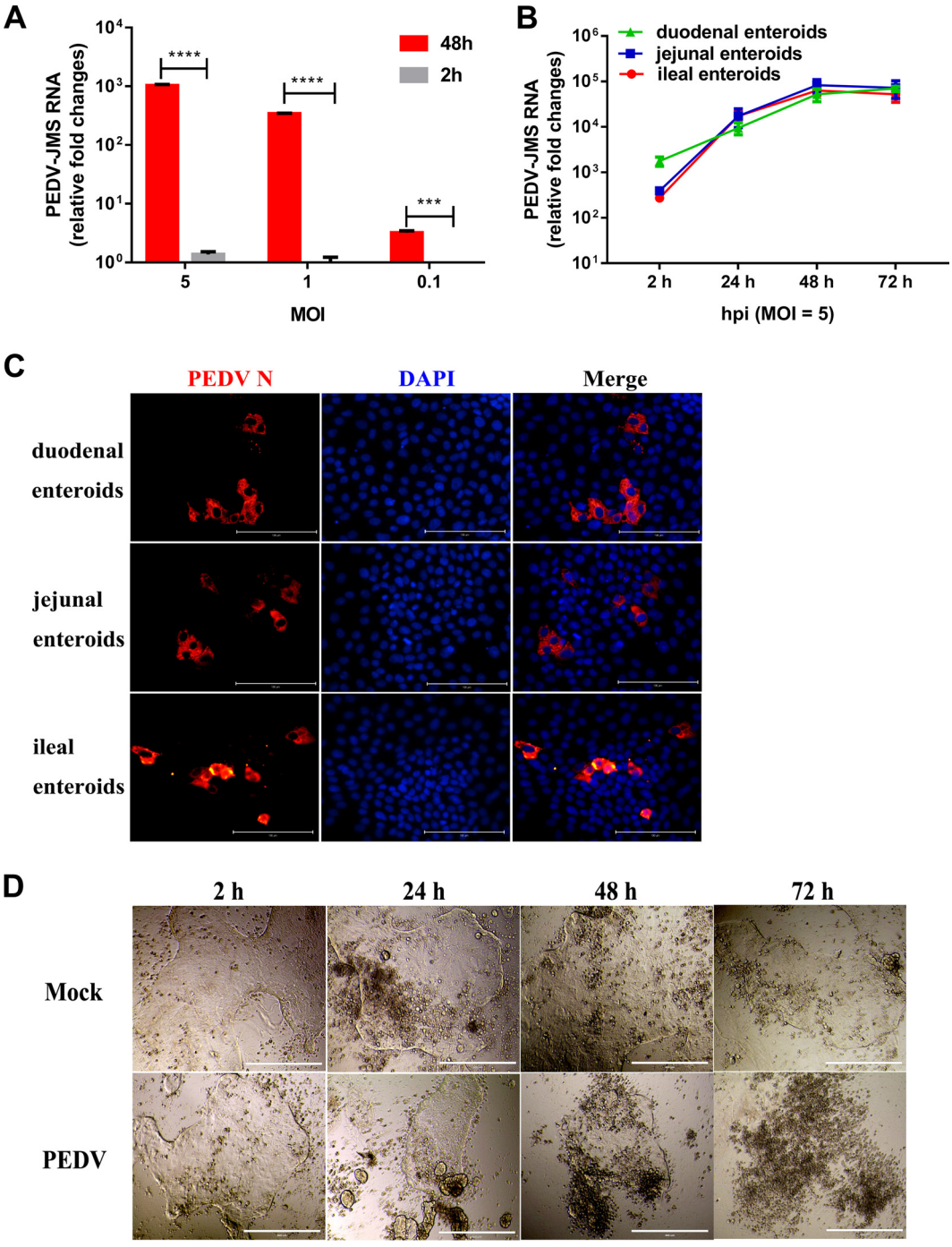

FIG 2 Detection of PEDV infection in porcine planar enteroids. (A) Detection of PEDV infection in planar ileal enteroids by RT-qPCR. Monolayers of porcine ileal enteroids were mock inoculated or inoculated with PEDV-JMS at the indicated MOIs for 2 h at 37°C. The inoculated enteroids were washed three times with PBS and harvested at 2 or 48 h postinfection. Total cellular RNA was extracted, and the number of PEDV genome copies was determined by RT-qPCR. The data are presented as the means of results from three wells for each treatment and time point. The error bars denote the standard error deviations. ***, $P < 0.005$; ****, $P < 0.001$. (B) Kinetic curve of PEDV replication in enteroids derived from duodenal, jejunal, or ileal crypts. Monolayer enteroids were inoculated with PEDV at an MOI of 5, and the level of PEDV infection at different time points postinfection was quantified by RT-qPCR. (C) Detection of PEDV infection in enteroids by a PEDV N protein IFA. Forty-eight hours after infection with PEDV at an MOI of 5, the enteroids were fixed with 4% paraformaldehyde, and the expression of PEDV N protein was detected with mouse anti-PEDV N mAb (red). DAPI was used to stain cellular nuclei (blue). (D) Bright-field images at various hours after PEDV-JMS infection (MOI = 5).

continued to deteriorate over time (Fig. 2D). These results indicate that PEDV successfully infects enteroids and establishes a productive infection.

Because intestinal enteroids contain multiple-cell-type compositions, we then took advantage of the multiple cellular phenotypes of intestinal enteroids and sought to clarify whether PEDV targets specific cell types in the porcine intestinal enteroids through double-immunofluorescence labeling (Fig. 3A). We detected PEDV infection in differentiated mature enterocyte cells that express villin, which serves as a surface marker for differentiated intestinal epithelial cells and is expressed in cells located in the brush border of the intestine (25, 26). Moreover, we observed PEDV infection (nucleocapsid positive) in Lgr5$^+$ stem cells, Ki-67-positive (proliferating) cells, and Muc2$^+$ goblet cells, although the number of PEDV-positive cells in the latter two cell populations was limited (Fig. 3A). These results indicate that PEDV infects multiple cell lineages, including stem cells and goblet cells. Thus, these data show that PEDV can infect enteroids, including enterocytes, stem cells, and goblet cells.

To further verify whether PEDV infects multiple cell lineages *in vivo*, we subjected ileal tissues collected from PEDV-infected piglets to immunohistochemistry staining. Consistent with data from previous reports, PEDV infection caused severe atrophic enteritis, and PEDV antigen-positive cells were largely located along the sides of villi, suggesting that PEDV successfully infects ileal tissue (Fig. 3B) (27). We also performed double-immunofluorescence staining of the same sample with anti-PEDV spike protein and anti-cell markers (villin, Lgr5, Ki-67, and Muc2) (Fig. 3C). As expected, villin, a marker of mature enterocytes, was present along the apical side of the intestinal villus, and PEDV infection was distributed throughout the villin-positive villi. PEDV infection was primarily located on the tip and waist of villi, and Lgr5-positive cells were primarily concentrated at the bottom crypt area of intestinal villi. We easily identified significant PEDV infection in Lgr5$^+$ cells in the crypt area (Fig. 3C), which indicates that PEDV infects Lgr5$^+$ crypt stem cells, as observed *in vitro* in enteroids. Unlike Lgr5 staining, which was concentrated in the bottom crypt, Ki-67-positive cells were distributed widely in the proliferative zone of the crypt and reached the waist area of villi (Fig. 3C). PEDV protein was occasionally observed in Ki-67$^+$ proliferating epithelial cells and to a lesser degree in Muc2$^+$ goblet cells (Fig. 3C). These results demonstrate that PEDV is capable of infecting multiple cellular lineages, including enterocytes, stem cells, and goblet cells, as observed *in vitro*. Thus, intestinal enteroids provide a unique platform for studying the multiple cellular targets of PEDV and the effect of PEDV infection on these various epithelial lineages.

PEDV preferentially infects ileal enteroids compared with colonoids. PEDV largely infects the villous epithelial cells of the small intestine *in vivo*, although restricted infection has also been observed in the colon (15). To recapitulate the segmental discrepancy of PEDV infection observed *in vivo*, we isolated crypt stem cells from ileal and colonic tissues from the same piglet. The stem cells from both ileal and colonic crypts expanded and differentiated into enteroids and colonoids, respectively (Fig. 1A and 4A), but the rates of intestinal organoid differentiation were not identical. Approximately 7 days were required for the ileal crypt stem cells to differentiate into enteroids, whereas the colonic crypt stem cells required a longer time (approximately 2 weeks) to differentiate into colonoids (Fig. 4A). Consistent with the segmental discrepancy of PEDV infection observed *in vivo* in the intestine, PEDV infected both ileal enteroids and colonoids but showed restricted infection in colonoids (Fig. 4B). The number of PEDV genome copies in colonoids at 72 hpi was increased only approximately 5-fold compared with that at 2 hpi, whereas the number of PEDV genome copies in ileal enteroids was substantially elevated from 24 to 72 hpi to reach values at 72 h that were 1,527-fold higher than those at 2 hpi. Consistent with the PEDV genome numbers, at 24 to 72 hpi at the same MOIs, ileal enteroids produced up to 44-fold more infectious particles than colonic enteroids (Fig. 4C). The discrepancy in infection between ileal enteroids and colonoids was further confirmed by a PEDV N protein IFA (Fig. 4D), and the results were consistent with the *in vivo* results: PEDV infection did not

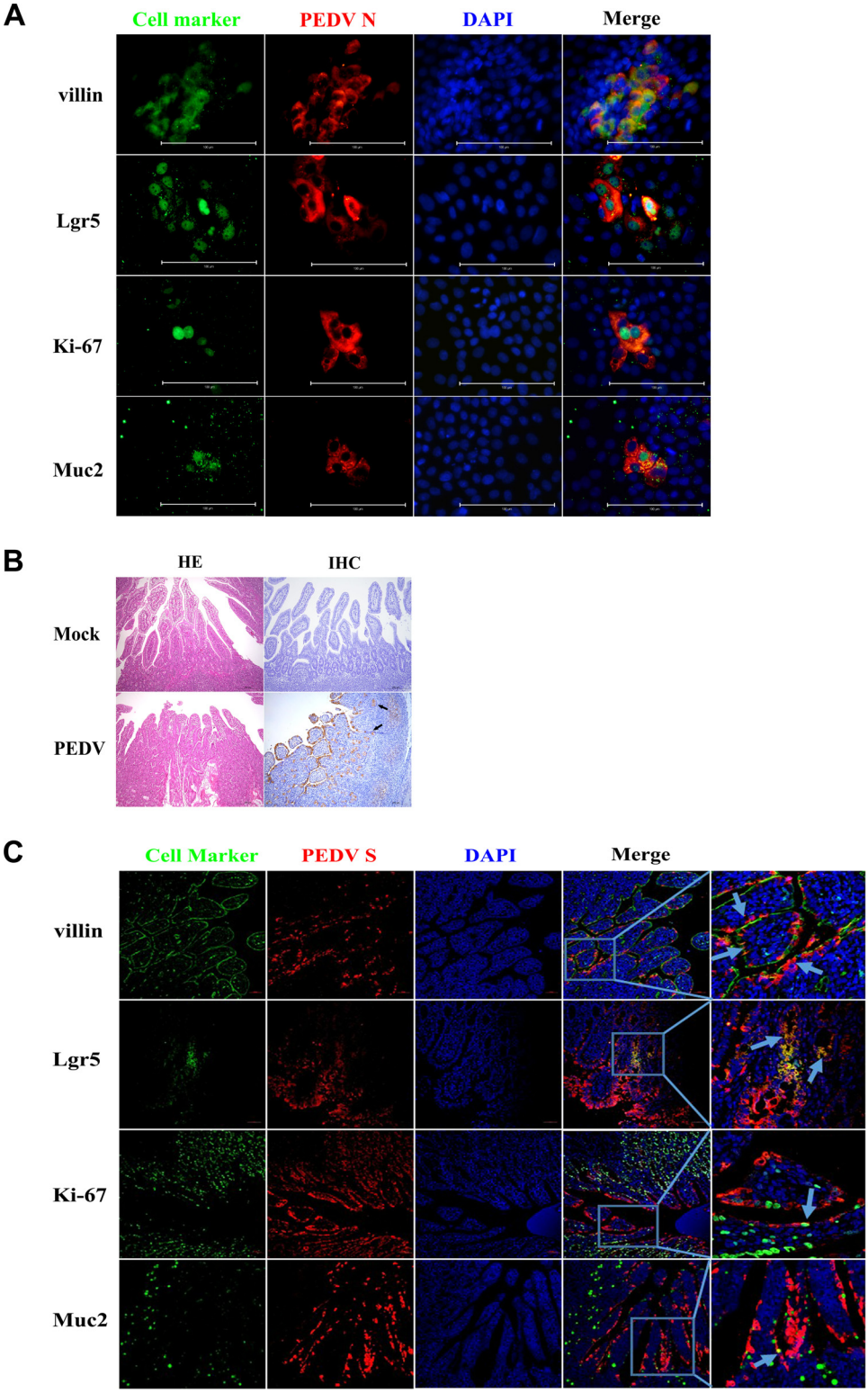

FIG 3 Identification of the phenotypes of cells infected by PEDV *in vitro* and *in vivo*. (A) Double-immunofluorescence labeling of ileal enteroids infected with PEDV-JMS at 48 hpi. Villin, Lgr5, Ki-67, and mucin 2 were used as enterocyte, intestinal stem cell, proliferating cell, and goblet cell markers (green), respectively. PEDV was labeled with anti-PEDV N protein antibody (red). DAPI was used for nuclear staining. Bar = 100 μm. (B) *In vivo* H&E staining and immunohistochemistry assay with an antibody to PEDV S protein. Samples (ileum) were collected from SPF piglets inoculated orally with mock DMEM or PEDV-JMS (black arrows). (C) *In vivo* double-labeling histoimmunofluorescence assay with antibodies, as described above for panel A. Samples (ileum) were collected from SPF piglets inoculated orally with PEDV. Specific cell marker (green) and PEDV S (red) double-labeled cells are indicated by light blue arrows. DAPI (blue) was used for nuclear staining. Bars = 50 μm.

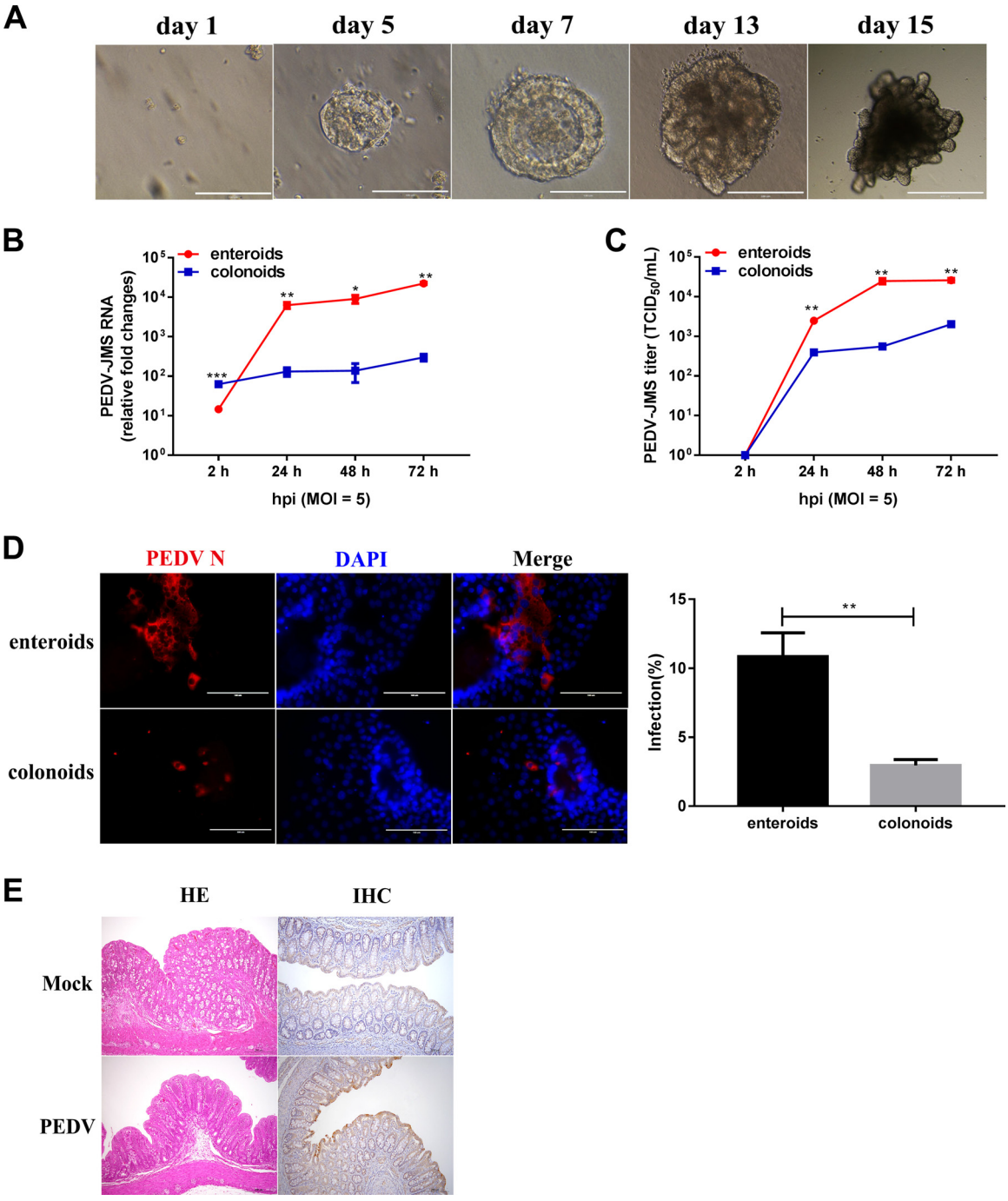

FIG 4 PEDV preferably infects ileal enteroids compared with colonoids. (A) Representative images of the time course of porcine colonoid development. Colonic crypts were isolated and differentiated into colonoids using the process used for the differentiation of ileal enteroids described in the legend of Fig. 1A. (B and C) Kinetic curve of PEDV-JMS replication in ileal enteroids or colonoids. Planar ileal enteroids or colonoids derived from the same piglet were infected with PEDV-JMS at an MOI of 5. The kinetics of PEDV production were determined by RT-qPCR (B) or titration (C). The data are presented as the means ± SEMs of results from three wells for each treatment and represent the results obtained for enteroids from two SPF piglets. The *P* values indicate the significance of the difference between ileal enteroids and colonoids. (D) Detection of PEDV infection in ileal enteroids or colonoids by an IFA. Planar ileal enteroids or colonoids were infected with PEDV at an MOI of 5, and the level of PEDV infection at 48 hpi was detected by staining with anti-PEDV N mAb. Representative IFA images were randomly selected from four fields per well, and PEDV$^+$ cells were counted. The results are presented in the right bar graph. (E) *In vivo* H&E staining and immunohistochemistry assay with an antibody to PEDV S protein. Samples (colon) were collected from SPF piglets inoculated orally with mock DMEM or PEDV-JMS. *, $P < 0.05$; **, $P < 0.01$; ***, $P < 0.005$.

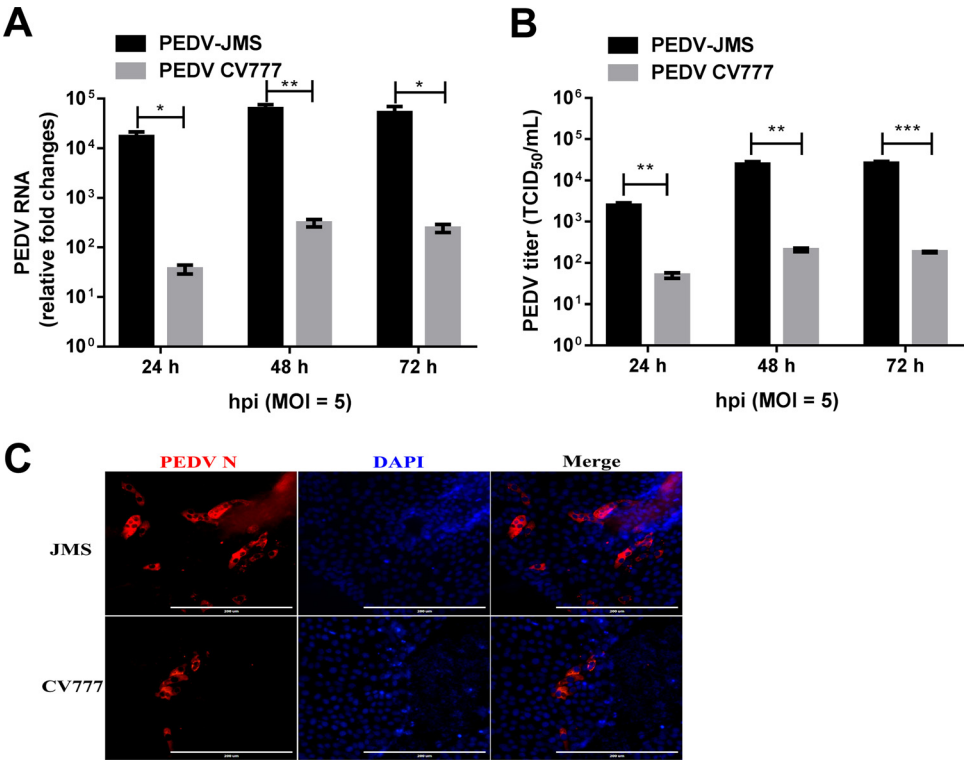

FIG 5 PEDV-JMS exhibits better infection in ileal enteroids than PEDV-CV777. (A and B) Viral replication kinetics of PEDV-JMS or PEDV-CV777 in ileal enteroids. Ileal enteroids were infected with PEDV-JMS or PEDV-CV777 at an MOI of 5, and PEDV production was determined at 24, 48, or 72 hpi by RT-qPCR (A) or viral titration (B). *, $P < 0.05$; **, $P < 0.01$; ***, $P < 0.005$. (C) Representative images of ileal enteroids infected with PEDV-JMS or PEDV-CV777. Ileal enteroids were infected with PEDV-JMS or PEDV-CV777 at an MOI of 5, and the level of PEDV infection was determined at 48 hpi by an anti-PEDV N IFA.

cause prominent pathological injury to colonic villi, and only a limited number of PEDV antigen-positive cells was detected in the colonic villi (Fig. 4E). Our results suggest that enteroids retain the internal region-specific identity among intestine segments. These data demonstrate that enteroid systems well mimic the events that occur during PEDV infection *in vivo*.

A clinical PEDV isolate shows better propagation in ileal enteroids than the cell-adapted strain CV777. The growth of clinical isolates of PEDV in cell lineages such as Vero E6 cells is typically challenging. Often, cell-adapted PEDV grows well in continuous cell lines, such as Vero E6 cells, after being subjected to multiple rounds of blind passaging in the cell line. We subsequently compared the replication of the clinical isolate PEDV-JMS in porcine ileal enteroids with that of the cell-adapted strain PEDV-CV777. After infection at equivalent MOIs, PEDV-JMS in ileal enteroids produced up to 473-fold-higher levels of viral genomes than those obtained with PEDV-CV777 throughout the study period (Fig. 5A). Consistent with the RNA results, PEDV-JMS produced higher viral titers in enteroids, yielding values that were 49- to 140-fold higher than those obtained with PEDV-CV777 (Fig. 5B), which indicated that the clinical isolate PEDV-JMS exhibits better infection in ileal enteroids than the cell-adapted strain CV777. PEDV N protein IFAs further confirmed that PEDV-JMS propagated better in enteroids than PEDV-CV777, even though both viruses infected enteroids (Fig. 5C). These data indicate that enteroids can be a good culture system for isolating clinical PEDV isolates.

PEDV infection suppresses the induction of innate IFN responses in enteroids. Recent studies have shown that PEDV infection inhibits the production of type I and III IFN in IEC lines such as IPEC-J2 (21). To verify whether PEDV infection inhibits the innate IFN responses in enteroids, we monitored the mRNA transcripts of type I IFN (IFN alpha

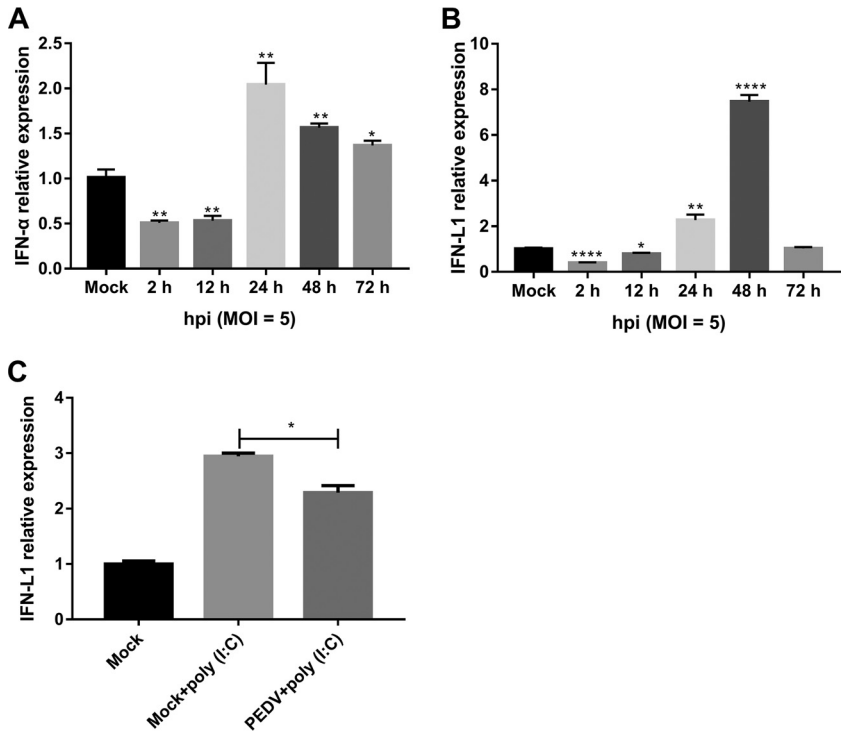

FIG 6 PEDV infection suppresses the induction of innate IFN responses in ileal enteroids. (A and B) PEDV infection suppresses cellular IFN production at the early stage of infection in ileal enteroids. The expression of IFN-α (A) or IFN-L1 (B) after PEDV-JMS infection (MOI = 5) was assessed by relative RT-qPCR. *, $P < 0.05$; **, $P < 0.01$; ****, $P < 0.001$ (versus mock). (C) Inhibition of poly(I·C)-elicited IFN-L1 production by PEDV-JMS in enteroids. Ileal enteroids were infected with PEDV-JMS at an MOI of 5 for 12 h and then stimulated with poly(I·C) for 12 h. Total cellular RNA was purified, and the mRNA level of IFN-L1 was quantified by RT-qPCR. The results are presented as the means ± SEMs ($n = 3$).

[IFN-α]) and type III IFN lambda 1 (IFN-L1) by reverse transcriptase quantitative PCR (RT-qPCR) in enteroids at various time points after infection with PEDV-JMS. Compared with the mock uninfected control, PEDV-JMS caused a rapid and substantial reduction in the expression of IFN-α and IFN-L1 transcripts, as observed at 2 and 12 hpi, and this decrease was followed by the induction of IFN expression after 24 hpi, indicating that PEDV infection inhibits the induction of type I and III IFN at the early stage of infection. However, the IFN-α and IFN-L1 expression kinetics were not identical (Fig. 6A and B): IFN-α expression peaked at 24 hpi, whereas IFN-L1 expression peaked at 48 hpi. To further verify that PEDV infection suppresses the induction of IFNs, we assessed IFN-L1 production after stimulating PEDV-infected enteroids at 12 hpi with poly(I·C) for 12 h. Stimulation with poly(I·C) substantially increased the expression of IFN-L1 in enteroids (Fig. 6C), which suggested that enteroids are capable of efficiently producing IFN-L1. In contrast, PEDV infection for 12 hpi significantly reduced the poly(I·C)-elicited production of IFN-L1 (Fig. 6C), which suggested that PEDV suppresses IFN production in enteroids. These findings indicate that intestinal enteroids are a suitable *ex vivo* model for the study of innate immunity in response to PEDV infection.

IFN-L1 induces potent ISG expression and inhibits PEDV infection in ileal enteroids. We and others have shown that compared with IFN-α, IFN-L1 selectively acts on IPEC-J2 cells and induces potent interferon-stimulated gene (ISG) expression (21, 28). To gauge the antiviral activities of type III and I IFNs against virus infection in enteroids, we initially monitored ISG expression in enteroids that had been primed for 24 h with either IFN-L1 or IFN-α. Both IFN-L1 and IFN-α elicited potent expression of interferon-stimulated gene 15 (ISG15) (Fig. 7A), MxA (Fig. 7B), 2′-5′-oligoadenylate synthetase-like protein (OASL) (Fig. 7C), and interferon-induced transmembrane protein 1 (IFITM1) (Fig. 7D) in a dose-dependent manner after stimulation. Consistent with the

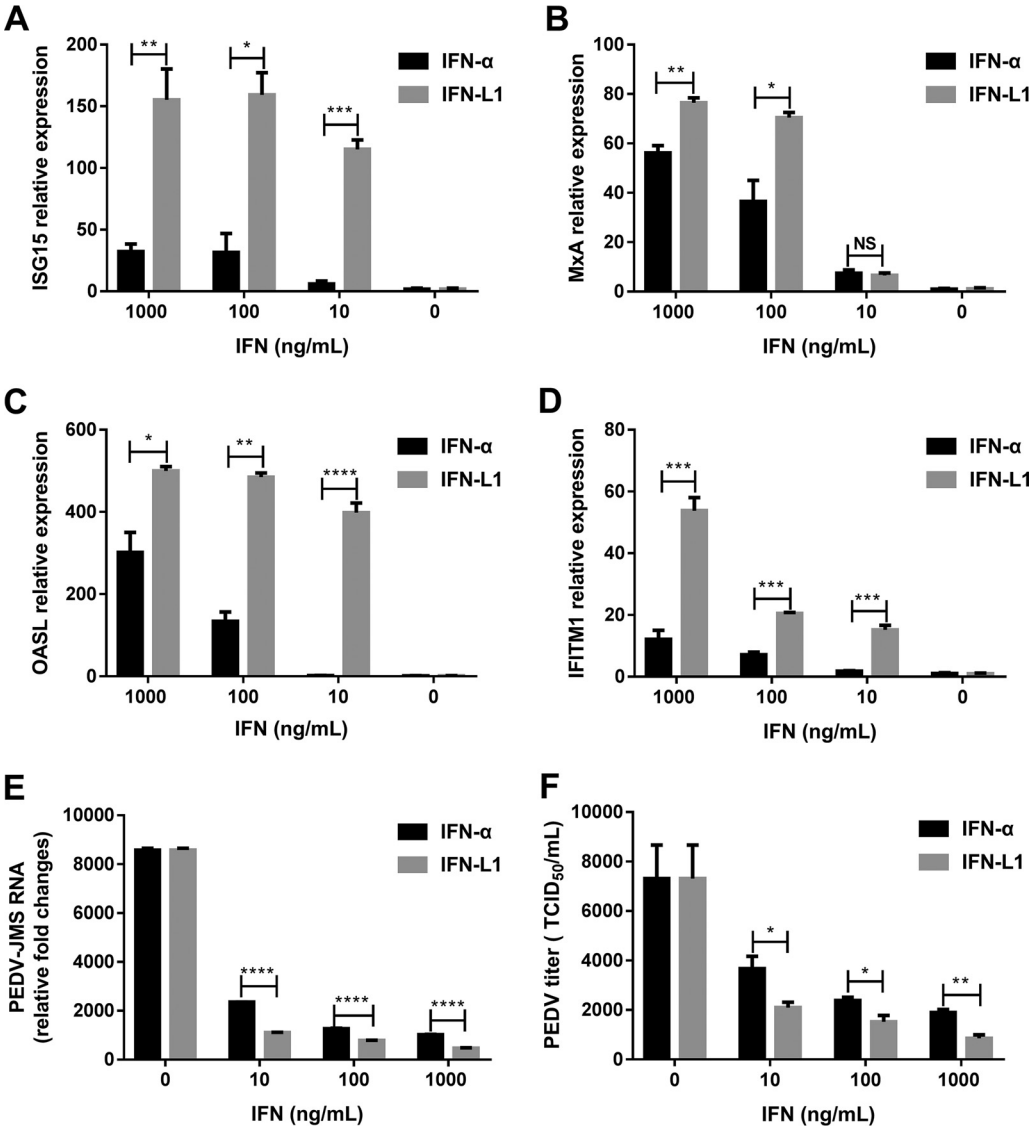

FIG 7 IFN-L1 selectively induces a substantial IFN antiviral response and inhibits PEDV infection in ileal enteroids compared with IFN-α. (A to D) ISG expression in ileal enteroids after IFN stimulation. Ileal enteroids were stimulated with IFN at the indicated concentrations for 24 h, and the mRNA levels of ISG15 (A), MxA (B), OASL (C), and IFITM1 (D) were quantified by RT-qPCR. (E and F) Inhibition of PEDV infection in ileal enteroids by IFN-L1 and IFN-α. Intestinal enteroids were primed with IFN for 24 h and infected with PEDV-JMS at an MOI of 1, and the PEDV genome numbers (E) and titers (F) at 48 hpi were determined by RT-qPCR and titration, respectively. The results are presented as the means ± SEMs ($n = 3$). *, $P < 0.05$; **, $P < 0.01$; ***, $P < 0.005$; ****, $P < 0.001$.

above-described results for IPEC-J2 cells, IFN-L1 induced significantly higher levels of ISG15, OASL, MxA, and IFITM1 in enteroids than IFN-α, regardless of the concentrations of IFNs (Fig. 7A to D). In agreement with the ISG expression profiles elicited by IFN-L1 and IFN-α, both IFN-L1 and IFN-α inhibited PEDV infection in enteroids in a dose-dependent manner, although IFN-L1 showed stronger antiviral activity against PEDV than IFN-α (Fig. 7E and F). These results demonstrate that IFN-L1 exhibits increased activity on enteroids compared to IFN-α. In summary, intestinal enteroids present a good *in vitro* model for evaluating the innate response to PEDV infection.

DISCUSSION

PEDV is primarily transmitted through the fecal-oral route and infects intestinal villous epithelial cells *in vivo* (12, 27). Current *in vitro* cell culture models of PEDV include Vero cells (29), MARC-145 cells (another monkey kidney cell line), HEK293 cells (30), and

IPEC-J2 cells (21, 31), and most of these are nonporcine intestinal epithelial cells and thus not the ideal *in vitro* cellular models for studying the interaction between PEDV infection and the host response due to interspecific variation. Although IPEC-J2 cells are a nontransformed porcine intestinal epithelial cell line, these cells lack the complexity of the cell types found in and the architecture of the intestinal epithelium and thus do not satisfactorily mimic the natural infection process. Intestinal enteroids represent a significant advantage over traditional *in vitro* models and provide a unique opportunity to explore host-pathogen interactions in an *in vitro* system that recapitulates the complicated cellularity of the GI tract. Although great progress has been achieved in generating human and mouse intestinal enteroids and using *ex vivo* systems to better understand the intestinal physiology and pathophysiology of enteric infection, previous studies have not investigated enteric viral infection in enteroids derived from porcine crypt stem cells. Here, we established a porcine enteroid culture system from crypt cells that contains enterocytes, enteroendocrine cells, goblet cells, Paneth cells, and stem cells and found that the proposed system well recapitulates the complex intestinal epithelium *in vivo* (Fig. 1). The porcine crypt enteroids derived from all three small intestinal regions were found to be permissive to infection by PEDV and provide a unique platform for studying intestinal physiology and a variety of biological aspects of porcine enteric pathogens.

The use of enteroids represents a significant advantage over traditional *in vitro* methods because they closely mimic the structure and function of the small intestine while maintaining the genetic identity of the host. Enteroids derived from crypt stem cells from different intestinal segments of the same donor allow assessment of the contributions of different intestinal segments to PEDV infection. Previous studies and our results have shown that PEDV largely infects the epithelial cells of the small intestine and occasionally infects colon epithelial cells (Fig. 2 to 4) (27, 32). In fact, we observed differential susceptibilities to PEDV infection between colonoids and ileal enteroids (Fig. 4B to D), indicating that the segment-specific difference is maintained *ex vivo* in enteroid cultures. These data illustrate the utility of the enteroid system for addressing fundamental aspects of PEDV that cannot be modeled using standard cell lines.

Due to their unique features, enteroids better mimic the multiple cell types of the intestinal epithelium *in vivo* than traditional cell line models. We observed that PEDV was capable of infecting goblet cells and stem cells in addition to the primary cellular target, villous mature enterocytes, in the enteroids, and this finding was confirmed *in vivo* in the PEDV-infected ileum (Fig. 3C). The intestinal epithelium is a rapidly self-renewing tissue, and the turnover rate for complete renewal is approximately 3 to 5 days (33). The Lgr5$^+$ stem cells in crypts are primarily responsible for replenishing the intestinal epithelium at a high rate of turnover. PEDV infection is cytolytic and causes acute necrosis of the infected enterocytes, leading to marked intestinal villous atrophy (12, 14, 15). Elucidating the effect of PEDV infection on crypt proliferation and differentiation has been a critical challenge. Only two previous reports have shown that PEDV infection causes a substantial increase in the number of Ki-67-positive cells and induces the localization of large numbers of Lgr5$^+$ cells in the crypt niches of the intestine of PEDV-infected pigs (13, 15). A previous study conducted by Jung and Saif showed that the numbers of Lgr5$^+$ cells and the proliferation of crypt cells are associated with piglet age, which is associated with susceptibility to PEDV infection (13). These results indicate that crypt stem cells are involved in the pathogenesis of PEDV infection. However, whether PEDV directly infects Lgr5$^+$ stem cells is unknown. Madson et al. previously visualized PEDV protein at the villus-crypt interface of the distal jejunum and ileum early during the infection process (32). Here, we directly observed PEDV proteins in Lgr5$^+$ cells and Ki-67$^+$ transit-amplifying cells in both ileal enteroids and infected ileal tissue. Enterocytes move on luminal surfaces from the bottom crypt area as they differentiate and mature, but further studies are needed to clarify whether the location and maturity of enterocytes influence the susceptibility of these cells to PEDV infection. In contrast to the previous *in vivo* study (27), we did not

observe a significant increase in the number of Ki-67$^+$ epithelial cells following PEDV infection in enteroids. Other factors might be involved in the increase in the number of Ki-67$^+$ epithelial cells during *in vivo* PEDV infection, and enteroids provide a good *in vitro* model to further address this question.

Goblet cells are simple columnar epithelial cells that constitute the primary cellular source of Muc2 mucins (34, 35). Mucins form an intestinal inner mucus layer, which serves as a physical barrier that effectively separates the commensal microbiota from the single epithelial cell layer and plays crucial roles in the maintenance of microbial homeostasis and the protection of epithelial cells from infection (36, 37). Jung et al. previously detected a PEDV antigen in goblet cells and demonstrated that PEDV infection caused a substantial reduction in the number of goblet cells in the small intestine (27, 38). In agreement with the previous *in vivo* results, we observed that PEDV infected goblet cells of enteroids *in vitro*. Another porcine alphacoronavirus, transmissible gastroenteritis virus (TGEV), reportedly binds to mucin on the apical membrane of intestinal cells, which allows TGEV to stay longer in the intestine and facilitates intestinal infection (39). However, whether PEDV takes advantage of mucin to facilitate the infection of goblet cells and the effect of PEDV infection on the functions of goblet cells remain unclear. In addition to the secretion of mucins, goblet cells play crucial roles in the presentation of oral antigens to the immune system (34). In the future, it will be very interesting to further explore the effect of PEDV infection on the functions of goblet cells by taking advantage of the enteroid model.

In summary, we show that porcine enteroids can be used to model the multicellular phenotype of the intestinal epithelium, which serves as the primary portal through which enteric viruses enter the hosts. Our findings provide important insights into events associated with PEDV infection and demonstrate that swine enteroids can be used as a unique model to define the complicated cross talk that exists between PEDV and the intestinal epithelium, which would undoubtedly have profound impacts on the clarification of PEDV pathogenesis. Intestinal enteroids also provide a platform for exploring the role of additional host factors in cellular tropism and can be used to isolate and grow previously uncultivable enteric viruses.

MATERIALS AND METHODS

Cell cultures. African green monkey kidney cells (Vero E6) were grown and maintained in Dulbecco's modified Eagle's medium (DMEM) supplemented with antibiotics (100 U/ml penicillin and 100 μg/ml streptomycin) and 10% heat-inactivated fetal bovine serum (FBS) (Gibco).

Virus stocks, titration, and infection of cells. The Vero cell-adapted PEDV-CV777 strain (GenBank accession no. KT323979) was propagated as previously described (40, 41). The PEDV-JMS strain (passage 6) was isolated and stocked by our laboratory, and the PEDV stock was prepared and titrated as described previously (22, 40). To assess the anti-PEDV activity of IFN-α and IFN-L1, cells were infected with PEDV after being primed with the indicated concentrations of IFN for 24 h. Samples were collected at the indicated times postinfection for the quantification of PEDV infection.

Porcine intestinal crypt isolation and 3D enteroid culture. Porcine intestinal crypts were prepared from specific-pathogen-free (SPF) 2- to 10-day-old piglets using previously described protocols, with minor modifications (11, 23). Briefly, the intestine was opened lengthwise and cut into 2-mm segments. The intestinal pieces were washed several times until the supernatant was clear, and the washed intestinal pieces were then suspended in gentle cell dissociation reagent (Stemcell, Canada) to dissociate the crypts. The pellets of the intestinal pieces were suspended in 10 ml of cold phosphate-buffered saline (PBS) with 0.1% bovine serum albumin (BSA) and antibiotics (penicillin-streptomycin) and passed through a 70-μm filter. The crypt pellets were harvested by centrifugation at 200 $\times$ *g* at 4°C for 5 min and resuspended in 10 ml of cold DMEM–F-12 medium. After counting, the intestinal crypts were resuspended with IntestiCult organoid growth medium (Stemcell, Canada) and Matrigel (BD Biosciences, USA) and seeded into a 48-well plate at a density of 50 crypts per well. The plate was incubated at 37°C for 10 min until the Matrigel solidified, and 300 μl of IntestiCult organoid growth medium was then added to each well. The plate was subsequently incubated at 37°C in a 5% CO_2 incubator, and the culture medium was exchanged every 3 to 4 days. The Institutional Animal Care and Use Committee of the Harbin Veterinary Research Institute approved all the protocols used for animal experiments in this study.

2D monolayer enteroid culture. Expanded 3D enteroids were recovered from Matrigel after 7 to 14 days of growth by the addition of ice-cold DMEM–F-12 medium, transferred into 15-ml tubes, and centrifuged at 250 $\times$ *g* at 4°C for 5 min. The enteroid pellet was incubated in 0.25% trypsin-EDTA (Gibco) for 5 min at 37°C and dissociated by repeated pipetting to obtain a single-cell suspension. DMEM–F-12 medium with 10% (vol/vol) FBS was added to the single-cell suspension, and the mixture was centrifuged at 800 $\times$ *g* for 5 min. The cell pellets were resuspended in complete IntestiCult organoid growth medium

TABLE 1 Primers for qPCR

Gene[a]	Primer direction	Primer sequence (5′–3′)
MxA	Forward	CACTGCTTTGATACAAGGAGAGG
	Reverse	GCACTCCATCTGCAGAACTCAT
ISG15	Forward	AGCATGGTCCTGTTGATGGTG
	Reverse	CAGAAATGGTCAGCTTGCACG
OASL	Forward	TCCCTGGGAAGAATGTGCAG
	Reverse	CCCTGGCAAGAGCATAGTGT
IFITM1	Forward	TGCCTCCACCGCCAAGT
	Reverse	GTGGCTCCGATGGTCAGAAT
IFN-α	Forward	CTGCTGCCTGGAATGAGAGCC
	Reverse	TGACACAGGCTTCCAGGTCCC
IFN-L1	Forward	CCACGTCGAACTTCAGGCTT
	Reverse	ATGTGCAAGTCTCCACTGGT
PEDV-CV777 ORF3	Forward	GCACTTATTGGCAGGCTTTGT
	Reverse	CCATTGAGAAAAGAAAGTGTCGTAG
PEDV-JMS ORF3	Forward	CACTTATTGGCAGGCTCTTT
	Reverse	CCATTGAGAAAAGAAAGTGTAGTAG
GAPDH	Forward	CCTTCCGTGTCCCTACTGCCAAC
	Reverse	GACGCCTGCTTCACCACCTTCT

[a]ORF3, open reading frame 3.

at room temperature (RT) and seeded at 50 enteroid cells per well in a Matrigel-precoated 96-well plate. After 3 days of differentiation, the planner monolayer 2D enteroids were ready for experiments.

Experimental infection of piglets. Four 10-day-old SPF piglets were randomly divided into two groups. The SPF piglets in group 1 were orally inoculated with 1.0 ml of 4.5×10^5 50% tissue culture infective doses ($TCID_{50}$) of the PEDV-JMS strain, and the SPF piglets in group 2 were inoculated with 1.0 ml of DMEM and served as uninfected controls. All clinical signs were recorded on a daily basis after virus infection, and all the piglets were euthanized at 4 days postinfection. The Animal Ethics Committee approved the protocol under approval no. Heilongjiang-SYXK-2006-032. Intestinal samples from the piglets were collected for pathological evaluation and assessment of PEDV infection.

RNA isolation and reverse transcriptase quantitative PCR. Total cellular mRNA was extracted using the Simply P total RNA extraction kit (BioFlux, China) according to the manufacturer's instructions. Total mRNA (1 μg) was reverse transcribed to cDNA using the PrimeScript II first-strand cDNA synthesis kit (TaKaRa, China), and relative gene expression levels were quantified by qPCR using SYBR green PCR mix (Life Technologies, USA) based on the cycle threshold ($\Delta\Delta C_T$) method (42). Glyceraldehyde-3-phosphate dehydrogenase (GAPDH) served as the internal control. The primers were designed using Primer Premier 5 software and are listed in Table 1.

H&E staining. Formalin-fixed ileum sections were serially dehydrated with 70%, 95%, and 100% ethanol; cleared in xylene; embedded in paraffin wax; and sectioned at a 4- to 6-μm thickness. After dewaxing in xylene and serially rehydration with 100%, 95%, and 70% ethanol, the ileum sections were stained with hematoxylin and eosin (H&E; Sigma-Aldrich) for histopathological evaluation and observed using a light microscope.

Immunohistochemistry. Ileum or colon tissue sections were deparaffinized in xylene and rehydrated with water containing descending concentrations (100%, 95%, and 70%) of ethanol. The slide was immersed in a citric acid (pH 7.4)–sodium citrate buffer solution (pH 8.0) at 121°C for 30 min for antigen retrieval. The tissues were rinsed with running tap water for 5 min and in PBS (Gibco) for 5 min, immersed in a 3% (vol/vol) H_2O_2–methanol solution for 30 min to block endogenous peroxidase activity, rinsed with running tap water for 5 min, and then blocked with 5% skim milk (Sigma-Aldrich, USA) in PBS for 30 min at room temperature. Mouse anti-PEDV spike protein monoclonal antibody (mAb) 6E5 (stocked in our laboratory) was diluted 1:200 in PBS. After overnight incubation at 4°C, the tissue sections were subjected to three 10-min washes with PBS. Subsequently, the slides were incubated with goat anti-rabbit secondary antibody in the dark for 30 min at room temperature, subjected to three 5-min washes with PBS, visualized rapidly using diaminobenzidine (DAB) (Sigma-Aldrich, USA), and counterstained with hematoxylin. The slides were then dehydrated with ascending concentrations (70%, 95%, and 100%) of ethanol, clarified in xylene, and mounted with Entellan mounting medium (Sigma-Aldrich, USA). Staining was observed using an optical microscope.

Immunofluorescence assay. Porcine intestinal enteroid monolayers were infected with PEDV-JMS at an MOI of 5. The level of PEDV infection at 48 h postinfection and the expression of differentiation markers were analyzed by an IFA as described previously (22). Briefly, porcine intestinal enteroid

monolayers were fixed with 4% paraformaldehyde (PFA) for 30 min at RT. After permeabilization with 0.2% Triton X-100, the cells were blocked with blocking buffer (PBS with 5% FBS and 5% skim milk), incubated with the primary antibodies for 2 h at 37°C, and stained with the secondary antibodies for 1 h at 37°C. The surface differentiation markers of intestinal epithelial cells were detected using primary anti-Ki-67 (1 μg/ml; Abcam, USA) for proliferative cells, anti-Lgr5 (1:50; Novus Biologicals, USA) for stem cells, anti-mucin 2 (1:50; Abcam, USA) for goblet cells, antivillin (1:100; Abcam, USA) and anti-chromogranin A (1:100; Santa Cruz, USA) for enteroendocrine cells, and antilysozyme (1:50; Santa Cruz, USA) for Paneth cells. Mouse anti-PEDV nucleocapsid mAb 2G3 was stocked in our laboratory (1:180 dilution). The cells were then labeled with secondary antibody conjugated to Alexa Fluor 488 donkey polyclonal antibody against rabbit IgG (1:1,000; Thermo Fisher Scientific, USA) or Alexa Fluor 546 goat anti-mouse IgG antibody (1:500; Thermo Fisher Scientific, USA). DAPI (4′,6-diamidino-2-phenylindole) (1:100; Sigma, USA) was used to stain cellular nuclei. The stained cells were visualized using an Evos FL Auto2 fluorescence microscope.

Representative sections of ileum or colon tissues were deparaffinized, rehydrated, heated for antigen retrieval, and blocked with 5% skim milk. Mouse anti-PEDV spike protein mAb 6E5 (1:200 dilution) was stocked in our laboratory. The surface differentiation markers of intestinal epithelial cells were stained as described above. The tissue sections were then rapidly washed three times in PBS, incubated with DAPI for 10 min at room temperature, and mounted. The slides were imaged using a Carl Zeiss microscope (LSM700; Carl Zeiss, Heidenheim, Germany) with the appropriate filter set.

Statistical analysis. All the results in the figures are presented, wherever appropriate, as the means ± the standard errors of the mean (SEMs) from three independent experiments and were analyzed using GraphPad Prism (GraphPad Software, Inc.). Differences were considered significant if the *P* value was <0.05.

ACKNOWLEDGMENTS

This work was supported by grants from the National Key R&D Program of China (2017YFD0502200) and the National Natural Science Fund (31772718).

REFERENCES

1. Peterson LW, Artis D. 2014. Intestinal epithelial cells: regulators of barrier function and immune homeostasis. Nat Rev Immunol 14:141–153. https://doi.org/10.1038/nri3608.
2. Moon C, Stappenbeck TS. 2012. Viral interactions with the host and microbiota in the intestine. Curr Opin Immunol 24:405–410. https://doi.org/10.1016/j.coi.2012.05.002.
3. Sato T, van Es JH, Snippert HJ, Stange DE, Vries RG, van den Born M, Barker N, Shroyer NF, van de Wetering M, Clevers H. 2011. Paneth cells constitute the niche for Lgr5 stem cells in intestinal crypts. Nature 469:415–418. https://doi.org/10.1038/nature09637.
4. Sato T, Vries RG, Snippert HJ, van de Wetering M, Barker N, Stange DE, van Es JH, Abo A, Kujala P, Peters PJ, Clevers H. 2009. Single Lgr5 stem cells build crypt-villus structures in vitro without a mesenchymal niche. Nature 459:262–265. https://doi.org/10.1038/nature07935.
5. Kovbasnjuk O, Zachos NC, In J, Foulke-Abel J, Ettayebi K, Hyser JM, Broughman JR, Zeng XL, Middendorp S, de Jonge HR, Estes MK, Donowitz M. 2013. Human enteroids: preclinical models of non-inflammatory diarrhea. Stem Cell Res Ther 4:S3. https://doi.org/10.1186/scrt364.
6. Lanik WE, Mara MA, Mihi B, Coyne CB, Good M. 2018. Stem cell-derived models of viral infections in the gastrointestinal tract. Viruses 10:E124. https://doi.org/10.3390/v10030124.
7. Saxena K, Blutt SE, Ettayebi K, Zeng XL, Broughman JR, Crawford SE, Karandikar UC, Sastri NP, Conner ME, Opekun AR, Graham DY, Qureshi W, Sherman V, Foulke-Abel J, In J, Kovbasnjuk O, Zachos NC, Donowitz M, Estes MK. 2016. Human intestinal enteroids: a new model to study human rotavirus infection, host restriction, and pathophysiology. J Virol 90:43–56. https://doi.org/10.1128/JVI.01930-15.
8. Luu L, Matthews ZJ, Armstrong SD, Powell P, Wileman T, Wastling JM, Coombes JL. 2018. Proteomic profiling of enteroid cultures skewed towards development of specific epithelial lineages. Proteomics 18:e1800132. https://doi.org/10.1002/pmic.201800132.
9. Barker N, Huch M, Kujala P, van de Wetering M, Snippert HJ, van Es JH, Sato T, Stange DE, Begthel H, van den Born M, Danenberg E, van den Brink S, Korving J, Abo A, Peters PJ, Wright N, Poulsom R, Clevers H. 2010. Lgr5(+ve) stem cells drive self-renewal in the stomach and build long-lived gastric units in vitro. Cell Stem Cell 6:25–36. https://doi.org/10.1016/j.stem.2009.11.013.
10. Ettayebi K, Crawford SE, Murakami K, Broughman JR, Karandikar U, Tenge VR, Neill FH, Blutt SE, Zeng XL, Qu L, Kou B, Opekun AR, Burrin D, Graham DY, Ramani S, Atmar RL, Estes MK. 2016. Replication of human noroviruses in stem cell-derived human enteroids. Science 353:1387–1393. https://doi.org/10.1126/science.aaf5211.
11. Ootani A, Li X, Sangiorgi E, Ho QT, Ueno H, Toda S, Sugihara H, Fujimoto K, Weissman IL, Capecchi MR, Kuo CJ. 2009. Sustained in vitro intestinal epithelial culture within a Wnt-dependent stem cell niche. Nat Med 15:701–706. https://doi.org/10.1038/nm.1951.
12. Lin CM, Saif LJ, Marthaler D, Wang Q. 2016. Evolution, antigenicity and pathogenicity of global porcine epidemic diarrhea virus strains. Virus Res 226:20–39. https://doi.org/10.1016/j.virusres.2016.05.023.
13. Jung K, Saif LJ. 2015. Porcine epidemic diarrhea virus infection: etiology, epidemiology, pathogenesis and immunoprophylaxis. Vet J 204:134–143. https://doi.org/10.1016/j.tvjl.2015.02.017.
14. Beall A, Yount B, Lin CM, Hou Y, Wang Q, Saif L, Baric R. 2016. Characterization of a pathogenic full-length cDNA clone and transmission model for porcine epidemic diarrhea virus strain PC22A. mBio 7:e01451-15. https://doi.org/10.1128/mBio.01451-15.
15. Jung K, Eyerly B, Annamalai T, Lu Z, Saif LJ. 2015. Structural alteration of tight and adherens junctions in villous and crypt epithelium of the small and large intestine of conventional nursing piglets infected with porcine epidemic diarrhea virus. Vet Microbiol 177:373–378. https://doi.org/10.1016/j.vetmic.2015.03.022.
16. Zhang J, Guo L, Yang L, Xu J, Zhang L, Feng L, Chen H, Wang Y. 2018. Metalloprotease ADAM17 regulates porcine epidemic diarrhea virus infection by modifying aminopeptidase N. Virology 517:24–29. https://doi.org/10.1016/j.virol.2018.02.001.
17. Zeng S, Zhang H, Ding Z, Luo R, An K, Liu L, Bi J, Chen H, Xiao S, Fang L. 2015. Proteome analysis of porcine epidemic diarrhea virus (PEDV)-infected Vero cells. Proteomics 15:1819–1828. https://doi.org/10.1002/pmic.201400458.
18. Ji CM, Wang B, Zhou J, Huang YW. 2018. Aminopeptidase-N-independent entry of porcine epidemic diarrhea virus into Vero or porcine small intestine epithelial cells. Virology 517:16–23. https://doi.org/10.1016/j.virol.2018.02.019.
19. Desmyter J, Melnick JL, Rawls WE. 1968. Defectiveness of interferon production and of rubella virus interference in a line of African green monkey kidney cells (Vero). J Virol 2:955–961.
20. Koh SY, George S, Brozel V, Moxley R, Francis D, Kaushik RS. 2008. Porcine intestinal epithelial cell lines as a new in vitro model for studying adherence and pathogenesis of enterotoxigenic Escherichia coli. Vet Microbiol 130:191–197. https://doi.org/10.1016/j.vetmic.2007.12.018.
21. Zhang Q, Ke H, Blikslager A, Fujita T, Yoo D. 2018. Type III interferon

restriction by porcine epidemic diarrhea virus and the role of viral protein nsp1 in IRF1 signaling. J Virol 92:e01677-17. https://doi.org/10.1128/JVI.01677-17.
22. Fu F, Li L, Shan L, Yang B, Shi H, Zhang J, Wang H, Feng L, Liu P. 2017. A spike-specific whole-porcine antibody isolated from a porcine B cell that neutralizes both genogroup 1 and 2 PEDV strains. Vet Microbiol 205:99–105. https://doi.org/10.1016/j.vetmic.2017.05.013.
23. van der Hee B, Loonen LMP, Taverne N, Taverne-Thiele JJ, Smidt H, Wells JM. 2018. Optimized procedures for generating an enhanced, near physiological 2D culture system from porcine intestinal organoids. Stem Cell Res 28:165–171. https://doi.org/10.1016/j.scr.2018.02.013.
24. Thorne CA, Chen IW, Sanman LE, Cobb MH, Wu LF, Altschuler SJ. 2018. Enteroid monolayers reveal an autonomous WNT and BMP circuit controlling intestinal epithelial growth and organization. Dev Cell 44:624.e4–633.e4. https://doi.org/10.1016/j.devcel.2018.01.024.
25. Cheung R, Kelly J, Macleod RJ. 2011. Regulation of villin by wnt5a/ror2 signaling in human intestinal cells. Front Physiol 2:58. https://doi.org/10.3389/fphys.2011.00058.
26. Landry C, Huet C, Mangeat P, Sahuquet A, Louvard D, Crine P. 1994. Comparative analysis of neutral endopeptidase (NEP) and villin gene expression during mouse embryogenesis and enterocyte maturation. Differentiation 56:55–65. https://doi.org/10.1046/j.1432-0436.1994.56120055.x.
27. Jung K, Annamalai T, Lu Z, Saif LJ. 2015. Comparative pathogenesis of US porcine epidemic diarrhea virus (PEDV) strain PC21A in conventional 9-day-old nursing piglets vs. 26-day-old weaned pigs. Vet Microbiol 178:31–40. https://doi.org/10.1016/j.vetmic.2015.04.022.
28. Li L, Fu F, Xue M, Chen W, Liu J, Shi H, Chen J, Bu Z, Feng L, Liu P. 2017. IFN-lambda preferably inhibits PEDV infection of porcine intestinal epithelial cells compared with IFN-alpha. Antiviral Res 140:76–82. https://doi.org/10.1016/j.antiviral.2017.01.012.
29. Lin CM, Hou Y, Marthaler DG, Gao X, Liu X, Zheng L, Saif LJ, Wang Q. 2017. Attenuation of an original US porcine epidemic diarrhea virus strain PC22A via serial cell culture passage. Vet Microbiol 201:62–71. https://doi.org/10.1016/j.vetmic.2017.01.015.
30. Zhang J, Guo L, Xu Y, Yang L, Shi H, Feng L, Wang Y. 2017. Characterization of porcine epidemic diarrhea virus infectivity in human embryonic kidney cells. Arch Virol 162:2415–2419. https://doi.org/10.1007/s00705-017-3369-2.
31. Xue M, Zhao J, Ying L, Fu F, Li L, Ma Y, Shi H, Zhang J, Feng L, Liu P. 2017. IL-22 suppresses the infection of porcine enteric coronaviruses and rotavirus by activating STAT3 signal pathway. Antiviral Res 142:68–75. https://doi.org/10.1016/j.antiviral.2017.03.006.
32. Madson DM, Arruda PH, Magstadt DR, Burrough ER, Hoang H, Sun D, Bower LP, Bhandari M, Gauger PC, Stevenson GW, Wilberts BL, Wang C, Zhang J, Yoon KJ. 2016. Characterization of porcine epidemic diarrhea virus isolate US/Iowa/18984/2013 infection in 1-day-old cesarean-derived colostrum-deprived piglets. Vet Pathol 53:44–52. https://doi.org/10.1177/0300985815591080.
33. Darwich AS, Aslam U, Ashcroft DM, Rostami-Hodjegan A. 2014. Meta-analysis of the turnover of intestinal epithelia in preclinical animal species and humans. Drug Metab Dispos 42:2016–2022. https://doi.org/10.1124/dmd.114.058404.
34. Pelaseyed T, Bergström JH, Gustafsson JK, Ermund A, Birchenough GMH, Schütte A, van der Post S, Svensson F, Rodríguez-Piñeiro AM, Nyström EEL, Wising C, Johansson MEV, Hansson GC. 2014. The mucus and mucins of the goblet cells and enterocytes provide the first defense line of the gastrointestinal tract and interact with the immune system. Immunol Rev 260:8–20. https://doi.org/10.1111/imr.12182.
35. Johansson ME, Hansson GC. 2016. Immunological aspects of intestinal mucus and mucins. Nat Rev Immunol 16:639–649. https://doi.org/10.1038/nri.2016.88.
36. Wlodarska M, Thaiss CA, Nowarski R, Henao-Mejia J, Zhang JP, Brown EM, Frankel G, Levy M, Katz MN, Philbrick WM, Elinav E, Finlay BB, Flavell RA. 2014. NLRP6 inflammasome orchestrates the colonic host-microbial interface by regulating goblet cell mucus secretion. Cell 156:1045–1059. https://doi.org/10.1016/j.cell.2014.01.026.
37. Johansson ME, Hansson GC. 2014. Is the intestinal goblet cell a major immune cell? Cell Host Microbe 15:251–252. https://doi.org/10.1016/j.chom.2014.02.014.
38. Jung K, Saif LJ. 2017. Goblet cell depletion in small intestinal villous and crypt epithelium of conventional nursing and weaned pigs infected with porcine epidemic diarrhea virus. Res Vet Sci 110:12–15. https://doi.org/10.1016/j.rvsc.2016.10.009.
39. Schwegmann-Wessels C, Zimmer G, Schroder B, Breves G, Herrler G. 2003. Binding of transmissible gastroenteritis coronavirus to brush border membrane sialoglycoproteins. J Virol 77:11846–11848. https://doi.org/10.1128/JVI.77.21.11846-11848.2003.
40. Sun D, Shi H, Guo D, Chen J, Shi D, Zhu Q, Zhang X, Feng L. 2015. Analysis of protein expression changes of the Vero E6 cells infected with classic PEDV strain CV777 by using quantitative proteomic technique. J Virol Methods 218:27–39. https://doi.org/10.1016/j.jviromet.2015.03.002.
41. Hofmann M, Wyler R. 1988. Propagation of the virus of porcine epidemic diarrhea in cell culture. J Clin Microbiol 26:2235–2239.
42. Schmittgen TD, Livak KJ. 2008. Analyzing real-time PCR data by the comparative C(T) method. Nat Protoc 3:1101–1108. https://doi.org/10.1038/nprot.2008.73.